arXiv:1708.01075v1 [cond-mat.mtrl-sci] 3 Aug 2017

# The role of van der Waals and exchange interactions in high-pressure solid hydrogen

Sam Azadi

*Royal School of Mines and the Thomas Young Centre,*

*Imperial College London, SW7 2AZ London,*

*School of Physics and Centre for Science at Extreme Conditions,*

*University of Edinburgh, Edinburgh EH9 3JZ, United Kingdom**

Graeme J. Ackland

*School of Physics and Centre for Science at Extreme Conditions,*

*University of Edinburgh, Edinburgh EH9 3JZ, United Kingdom*

(Dated: March 27, 2018)

## Abstract

We investigate the van der Waals interactions in solid molecular hydrogen structures. We calculate enthalpy and the Gibbs free energy to obtain zero and finite temperature phase diagrams, respectively. We employ density functional theory (DFT) to calculate the electronic structure and Density functional perturbation theory (DFPT) with van der Waals (vdW) functionals to obtain phonon spectra. We focus on the solid molecular $C2/c$, $Cmca$-12, $P6_3/m$, $Cmca$, and $Pbcn$ structures within the pressure range of $200 < \mathrm{P} < 450$ GPa. We propose two structures of the $C2/c$ and $Pbcn$ for phase III which are stabilized within different pressure range above 200 GPa. We find that vdW functionals have a big effect on vibrations and finite-temperature phase stability, however, different vdW functionals have different effects. We conclude that, in addition to the vdW interaction, a correct treatment of the high charge gradient limit is essential. We show that the dependence of molecular bond-lengths on exchange-correlation also has a considerable influence on the calculated metallization pressure, introducing errors of up to 100GPa.

## I. INTRODUCTION

Determining the phase diagram of high-pressure hydrogen is one of the great challenges of condensed matter physics. Since 1935, when it was predicted that molecular solid hydrogen would become a metallic atomic crystal at 25 GPa[1] high-pressure hydrogen has been studied intensively by theory and experiment. It was also predicted theoretically the possible existence of room-temperature superconductivity[2] and metallic liquid ground state[3]. Additional interests rise from the relevance of solid hydrogen to astrophysics[4,5].

Early infrared (IR) and Raman measurements at low temperature suggested the existence of three solid-hydrogen phases[4]. Phase I, which is stable up to 110±5 GPa, is a molecular solid composed of quantum rotors arranged in a hexagonal close-packed structure. Phase I spans a wide pressure-temperature (P-T) range. Hence the physical properties of phase I of hydrogen evolve extensively as the solid becomes nine times denser. It has been accepted that the melting curve of hydrogen exhibits a maximum below 130±10 GPa at around 1000±100 K[6–8,14]. Extrapolating the existing data to pressures larger than 250 GPa predicts room temperature melting at P > 300±50 GPa, but thermodynamics requires that the melt line will become shallower above the high-entropy phase IV[39]. Changes in the low-frequency regions of the Raman and infrared spectra imply the existence of phase II, also known as the broken-symmetry phase, above 110±5 GPa. Phase II is observed at temperatures below 100±20K. The appearance of phase III at 150 GPa and below room temperature is accompanied by a large discontinuity in the Raman spectrum and a strong rise in the IR spectral weight of molecular vibrons[10,62]. Phase IV, characterized by the two vibrons in its Raman spectrum, was recently discovered at 300 K and pressures above 230 GPa[11–13]. Another new phase has been found at pressures above 200 GPa and higher temperatures (for example, 480 K at 255 GPa)[14]. This phase is thought to meet phases I and IV at a triple point, near which hydrogen retains its molecular character. The most recent experimental results[15] indicate that $H_2$ and hydrogen deuteride at 300 K and pressures greater than 325 GPa transform to a new phase V, characterized by substantial weakening of the vibrational Raman activity. Other features include a change in the pressure dependence of the fundamental vibrational frequency and the partial loss of the low-frequency excitations.

Although it is very difficult to reach the hydrostatic pressure of more than 400 GPa at which hydrogen is normally expected to metallize, some experimental results have been in-

terpreted as indicating metallization at room temperature below 300 GPa[11]. However, other experiments show no evidence of the optical conductivity expected of a metal at any temperature up to the highest pressures explored[16]. Experimentally, it remains unclear whether or not the molecular phases III and IV are metallic, although it has been suggested that phase V may be non-molecular (atomic)[15]. Metallization is believed to occur either via the dissociation of hydrogen molecules and a structural transformation to an atomic metallic phase[11,17], or via band-gap closure within the molecular phases[18,19]. In this work we investigate the influence of van der Waals interactions on the metallization by performing finite temperature phase diagram calculations for insulator and metallic molecular structures.

The phase diagram of high-pressure solid hydrogen has mainly been investigated using density functional theory (DFT) with local and semi-local exchange-correlation (XC) functionals[20–29,38]. In particular, DFT with generalized gradient approximation (GGA) functionals has been widely applied to search for candidate low-energy crystal structures and to calculate their vibrational properties. Recently, DFT-GGA was used to reinterpret the IR spectrum of hydrogen-deuterium mixtures in molecular structures[30,31], and it has been found that the isotope effect leads to a completely different spectroscopic signal in hydrogen-deuterium mixtures. More accurate quantum Monte Carlo methods[32–34] are employed to calculate the static phase diagram[35,36] and excitonic and quasi-particle band gaps for molecular phases[37]. Just recently an interesting classical thermodynamic model that reproduces the main features of the solid hydrogen phase diagram has been introduced[39]. It was shown that the general structure types, which are found by electronic structure calculations and the quantum nature of the protons, can also be understood from a classical viewpoint.

The relative contribution of the van der Waals (vdW) interactions to the cohesive properties of the various solid molecular structures of high-pressure hydrogen has not been understood. First principles study of ice phase diagram provides an important consequence, likely to be of relevance to hydrogen-rich molecular crystals in general, which is that transition pressures obtained from DFT-XC which neglect vdW forces are greatly overestimated[40]. We have recently studied the phase diagram of compressed crystalline benzene using modern vdW and GGA density functionals[41]. We found that the vdW forces play crucial role in prediction of phase stability and transition pressure in crystalline benzene. Considering the aforementioned results for ice and crystalline benzene, it may be expected that the

vdW interactions are important in phase diagram calculations of low-Z hydrogen-dominant molecular crystals. Similar to other rare gases, simple $H_2$ molecules are weakly bounded due to vdW forces in ambient conditions. A detailed study of the helium-nitrogen system in a diamond-anvil cell using synchrotron X-ray diffraction, Raman scattering and optical microscopy, indicates a novel class of vdW compounds that are formed only at high pressures[42]. Theoretical study of liquid-liquid insulator-metal-transition phase boundaries for high-pressure deuterium[43] predicts that the pressure-temperature phase diagram results which are simulated by vdW functionals are in better agreement with experiment comparing with conventional density functionals. Therefore, we believe that it is important to understand the contribution of vdW interactions in static and dynamic phase diagrams of high-pressure solid molecular hydrogen.

The main purpose of current work is to study the role of vdW forces in the properties of molecular phases of high-pressure solid hydrogen. We calculate enthalpy-pressure static phase diagram and also the Gibbs free energy dynamic phase diagram up to room temperature. We employ two widely used vdW functionals of vdW-DF1[44,45] and vdW-DF2[46] and compare them with the results from conventional DFT functionals. Although these vdW functionals are tested on a broad range of materials including traditional metals, ionic compounds, and insulators[47,48], they were not employed before to calculate the finite-temperatures phase diagram of high-pressure solid hydrogen. We consider five specific molecular structures with space groups $P6_3/m$, $C2/c$, $Pbcn$, $Cmca$-12, and $Cmca$ within pressure range between 200 to 400 GPa. These structures were predicted by the *ab initio* random structure searching method[20]. According to those calculations, the $C2/c$ and $Pbcn$ structures are candidates for phases III and IV, respectively. The $C2/c$ structure includes weakly-bonded nearly graphene-like layers, while the $Pbcn$ phase adopts two different layers of nearly graphene-like three-molecule rings with elongated $H_2$ molecules and unbound $H_2$ molecules[12,20,23]. The $Cmca$-12 structure is similar to $C2/c$ but slightly denser and has a much smaller metalization pressure[35]. The $Cmca$ phase shows weaker molecular bonds than $C2/c$ and $Cmca$-12 and is the only metallic molecular phase within the studied pressure range. The structure of the $P6_3/m$ differs from the other layered phases. In this phase three quarters of the $H_2$ molecules lie flat in the plane and one quarter lie perpendicular to the plane. More recently, several other structures involving small symmetry-breaking distortions from $Pbcn$ have been proposed for Phase IV, but molecular dynamics simula-

tions at the temperatures where Phase IV is observed show that the unbound molecules rotate, increasing the time-averaged symmetry to $P6/mmm$[23,39,66,67]. With the PBE functional, further small distortions mean that the lowest known energy candidate for phase II is $P2_1/c$[65] and for phase III $P6_122$[63] and $C2/c-24$[65] below and above 200GPa respectively. With PBE the $Cmca$ phase is stabilised well into the pressure range where it has been ruled out experimentally.

Comparison between experiment and theory is typically done by comparing at the same pressure. However it is important to note that neither experiment nor theory is very reliable in measuring pressures. Experimental pressures are estimated with respect to the diamond absorption edge, a scale which has been frequently revised by tens of GPa[49]. The natural variable for quantum calculations is volume, with pressure being a calculated quantity. Standard DFT codes calculate the differential of the energy with respect to an affine rescaling of the simulation cell, neglecting zero point contribution and the different compressibility of inter- and intramolecular regions. Consequently experimental and theoretical measures are highly self-consistent, but comparing the two is dangerous.

Crystal structure and hydrogen positions in the primitive unit-cell are the fundamental inputs for *ab initio* phase diagram calculations. Due to lack of any established experimental structure determination, there is no option but to use structures predicted by DFT. Most of the structures have been predicted by Perdew-Burke-Ernzerhof (PBE)[51] exchange correlation (XC) functionals[20,21] which has become the *de facto* standard in structure searching packages. It is now generally accepted that DFT results for high-pressure hydrogen strongly depend on the choice of exchange-correlation functional[26,29,38] and although PBE performs well in identifying candidate structures, it is poor at describing the relative energies of configurations and the properties of the molecular bond[26]. The sensitivity to choice of DFT-XC functional depends on the property being studied, and serious doubts about the accuracy of the results persist. Is the pressure calculated correctly? How do the interatomic interaction energy, the bond-stretch energy, the phase diagram, the metallization mechanism, and the phonon spectrum depend on the approximation used for the XC functional? How accurate should we expect DFT calculations of measured quantities such as infrared (IR) and Raman spectra to be? Answering these questions is necessary to assess the reliability of the many existing DFT simulations of high-pressure solid hydrogen. In this work, we examine the accuracy of non-local vdW functionals in prediction of the properties of high-pressure solid hydrogen.

The paper is organized as follows. Section II describes the details of our vdW-DF calculations. The static and dynamic phase diagrams and also calculated IR intensities are discussed in Sec. III. Section IV concludes.

## II. COMPUTATIONAL DETAILS

Given that the energy differences between solid hydrogen molecular structures are small, the calculations must be performed with the highest possible numerical precision. Our DFT calculations were carried out within the pseudopotential and plane-wave approach using the latest version of Quantum ESPRESSO suite of programs[50]. Our DFT calculations used non-relativistic norm conserving pseudopotentials which were obtained by the Perdew-Burke-Ernzerhof (PBE)[51] exchange correlation functionals. We used a basis set of plane waves with an energy cutoff 80 Ry. Geometry and cell optimisations employed a dense $16 \times 16 \times 16$ **k**-point mesh. The quasi-Newton algorithm was used for cell and geometry optimisation, with convergence thresholds on the total energy and forces of 0.01 mRy and 0.1 mRy/Bohr, respectively, to guarantee convergence of the total energy to less than 1 meV/proton and the pressure to less than 0.1 GPa/proton.

Vibrational frequencies and phonon spectra were calculated using density-functional perturbation theory as implemented in Quantum ESPRESSO[50]. We use quasi-harmonic approximation to calculate the vibrational free energy[52]:

$$F_{ph}(T,V) = k_B T \sum_{i,\mathbf{q}} ln\{2sinh[\hbar\omega_{i,\mathbf{q}}(V)/2k_B T]\}, \tag{1}$$

where $k_B$, $V$, and $\omega_{i,\mathbf{q}}$ are Boltzmann constant, unit cell volume, and eigenvalue of the phonon Hamiltonian, respectively. The zero point (ZP) pressure is included in our phase diagram calculations by $P_{ZP} = -(\partial E_{ZP}/\partial V)$, where the $E_{ZP}$ per proton at a specific cell volume $V$ was estimated within the quasi-harmonic approximation: $E_{\rm ZP}(V) = \hbar\overline{\omega}/2$, where $\overline{\omega} = \sum_{\mathbf{q}} \sum_{i=1}^{N_{\rm mode}} \omega_i(\mathbf{q})/(N_{\mathbf{q}} N_{\rm mode})$. $N_{\rm mode}$ and $N_{\mathbf{q}}$ are the numbers of vibrational modes in the simulation cell and phonon wave vectors $\mathbf{q}$, respectively, and the summation over $\mathbf{q}$ includes all **k**-points on a $2 \times 2 \times 2$ grid in the Brillouin zone.

Our electronic structure and lattice dynamic results are calculated by vdW-DF1[44] and vdW-DF2[46] functionals. The Slater exchange and Perdew-Wang (PW)[53] correlation functionals are used in both vdW-DF1 and vdW-DF2 which means the correlation energy is

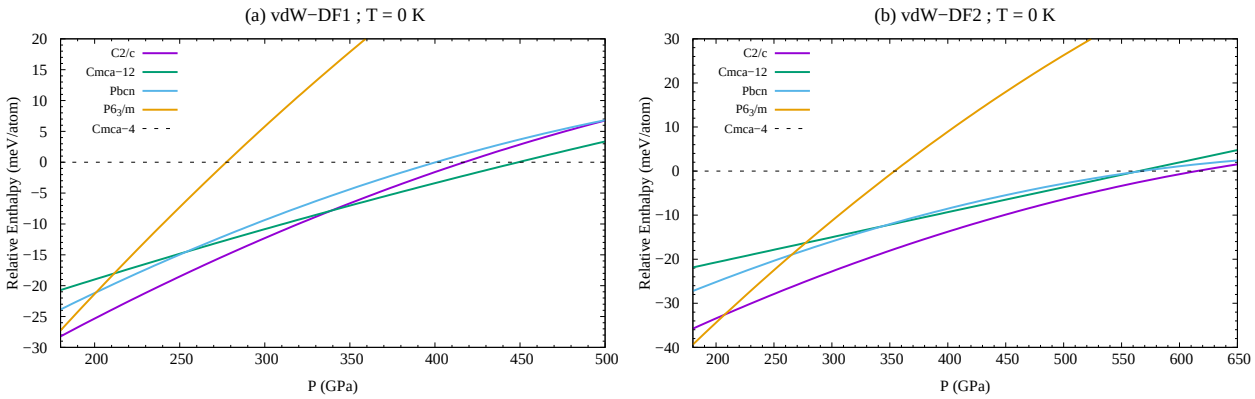


FIG. 1. (Color online) Relative enthalpy per atom as a function of pressure calculated using two different vdW functionals of vdW-DF1 and vdw-DF2. The static lattice (no phonon contributions) enthalpies of molecular crystal structures are presented relative to the enthalpy of the metallic *Cmca* structure.

approximated by local density approximation (LDA). In vdW-DF1 the gradient correction on exchange energy uses the revised version of PBE[54], whereas vdW-DF2 uses an optimized version of PW86[55] which is named PW86R[56]. These functionals use different kernel for non-local energy term which accounts approximately for the non-local electron correlation effects. The non-local term is obtained using a double space integration, which represents an improvement compared to local or semi-local functionals, especially in the case of layered structures[57].

## III. RESULTS AND DISCUSSION

### A. Static enthalpy-pressure phase diagram

Figure 1 illustrates static lattice enthalpy-pressure phase diagram calculated using the vdW-DF1 and vdW-DF2 functionals. According to our vdW-DF1 results the $C2/c$, $Cmca-12$, and metallic $Cmca$ phases are stable in the pressure ranges $<$ 200-340, 340-450, and $>$ 450 GPa, respectively. Our vdW-DF2 calculations predict that the $P6_3/m$ is stable below 210 GPa and the $C2/c$ is the most stable insulator phase until it transits to metallic $Cmca$ at pressure of 625 GPa. The relative stability of phases predicted by vdW-DF1 and vdW-DF2 is not similar. The vdW-DF1 and vdW-DF2 functionals predict that the molecular insulator to molecular metallic phase transition occurs at pressures 450, and 625 GP, respectively. Our

static enthalpy-pressure phase diagram obtained by vdW functionals differ from the previous results which are calculated by conventional DFT functionals[29]. PBE static lattice phase diagram predicts that the $P6_3/m$, $C2/c$,$Cmca$-12, and metallic $Cmca$ phases are stable in the pressure ranges $<$ 110, 110245, 245370, and $>$ 370 GPa, respectively. The semi-local Becke-Lee-Yang-Parr (BLYP) functional[58] enthalpy-pressure phase diagram indicates that the $P6_3/m$, $C2/c$,$Cmca$-12, and metallic $Cmca$ phases are stable in the pressure ranges of $<$ 160, 160370, 370430, and $>$ 430 GPa, respectively. Calculations using Local density approximation and PBEsol[59] also give diverse properties[38].

It has been proven that DFT electronic structure results in the case of high-pressure solid molecular hydrogen dramatically depend on the XC functional. In our previous work[29], we argued that the self-interaction (XC-SI) error present in the XC functionals plays crucial role in the study of $H_2$ systems. For instance, the XC-SI errors of the LDA, GGA, and BLYP total energies of a single $H_2$ molecule are 1.264, -0.126, and 0.0846 eV, respectively[60]. These values are more than two orders of magnitude larger than the conventional DFT enthalpy differences between the crystal structures of high-pressure solid hydrogen. Consequently DFT is highly dependent on cancellation of XC-SI errors: this is reasonable when comparing different molecular structures

The XC energy in vdW functionals, in general, can be expressed as: $E_{XC} = E_X^{GGA} + E_C^{LDA} + E_C^{non-local}$ where the $E_X^{GGA}$ is revPBE[54] and PW86R[56] for vdW-DF1 and vdW-DF2, respectively. The non-local part of correlation energy $E_C^{non-local}$ by definition does not suffer from the Coulomb self-energy of each electron. The local correlation energy $E_C^{LDA}$ is identical in vdW functionals considered in this work. Hence, the XC-SI errors of vdW-DF1 and vdW-DF2 are mostly related to the X-SI errors. It was reported that[61] the PW86 functional, shows the most consistent agreement with exact-exchange Hartree-Fock (HF) interaction energies for $H_2$ clusters. In the next section we discuss the overall behaviour of vdW-DF1 and vdW-DF2 for large density limit. It has been comprehensively discussed that properties such as molecular bond-length and interactions energies calculated by vdW-DF2 are improved[61]. However, at this stage we can not comment that this improvement is due to a lower SIE rather than other limits being obeyed. The study of SIE in DFT-XC functional demands a separate work.

To obtain a deep understanding of the static phase diagram and also for comparing our results with experiment, we calculate pressure-density equation of state using vdW-

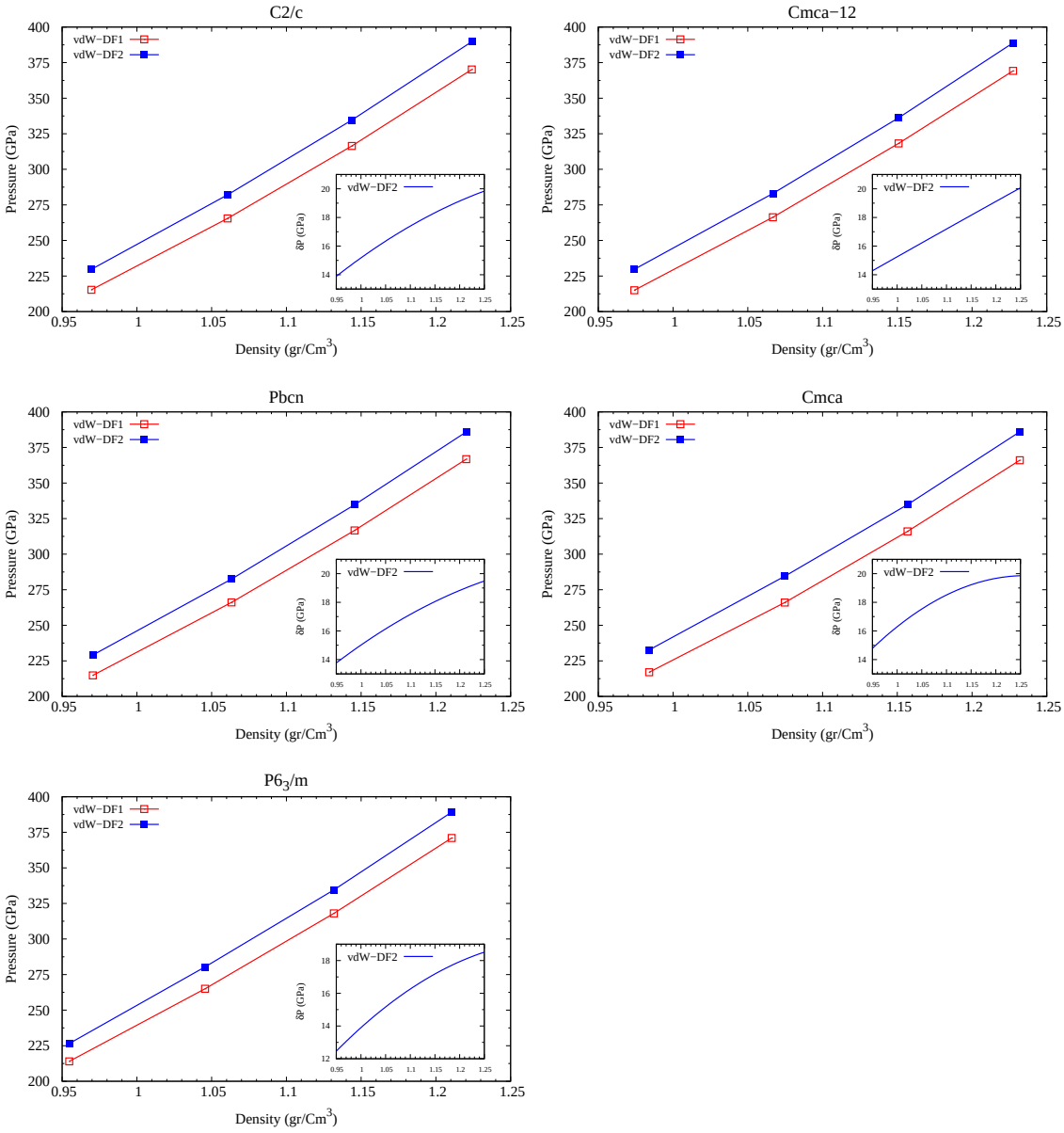


FIG. 2. (Color online) Pressure-density equation of state for the $C2/c$, $Cmca$-12, $Pbcn$, $Cmca$, and $P6_3/m$ phases calculated using vdW-DF1 and vdW-DF2 functionals. The inset shows evolution of $\delta$P, the difference between vdW-DF2 pressure and vdW-DF1 pressure, as a function of density. At a fixed density, vdW-DF2 predicts larger pressure than vdW-DF1.

DF1 and vdW-DF2. Figure2 illustrates pressure-density equation of state for the $C2/c$, $Cmca$-12, $Pbcn$, $Cmca$, and $P6_3/m$ molecular structures which are obtained by vdW-DF1 and vdW-DF2 functionals. Insets show the difference between pressure calcation at same density ($\delta P$), which increases with density and for all the studied structures. $\delta P$ is in the range 10-20GPa, and vdW-DF2 gives systematically larger pressures than vdW-DF1.

### B. Lattice dynamics and Bondlengths

Figure 3 illustrates phonon density of states (DOS) of the $C2/c$, $Pbcn$, $Cmca$-12, $P6_3/m$, and $Cmca$ structures which are obtained by vdW-DF1 and vdW-DF2 at four different pressures. Both vdW functionals predict that in all the studied molecular structures the phonon dispersion increases by increasing the pressure. The vibron frequencies predicted by vdW-DF1 are smaller than vdW-DF2. This difference is strongly related to the optimized $H-H$ molecular bond-length (BL) predicted by vdW functionals. Precise values of optimized molecular bond-length for all the studied structures, which are calculated by vdW-DF1 and vdW-DF2 at same density, are presented in table I, respectively.

In the primitive unit cell of $C2/c$ there are twelve $H_2$ molecules with two kinds of $H-H$ molecular bond-length named BL1 and BL2 in figure 4. The $C2/c-$BL1 which is shorter than $C2/c-$BL2 corresponds to higher vibron frequencies. vdW-DF1 and vdW-DF2 produce different results for the $C2/c-$BL1 and $C2/c-$BL2. According to vdW-DF1 results both $C2/c-$BL1 and $C2/c-$BL2 increase with density, whereas vdW-DF2 predict that $C2/c-$BL1 and $C2/c-$BL2 slightly decrease by increasing the pressure (Table I). The $C2/c-$BL1 and $C2/c-$BL2 obtained by vdW-DF1 are larger than those calculated by vdW-DF2 at the same density. Therefore, vdW-DF2 functional predict higher frequency vibrons. Same argument can be applied on the $Cmca-12$ phase. The difference between $Cmca$-12$-$BL1 and $Cmca$-12$-$BL2 is larger than the difference between $C2/c-$BL1 and $C2/c-$BL2. Hence, the $Cmca$-12 phonon vdW's DOS results predict lower frequencies for vibrons than $C2/c$. $Cmca$-12$-$BL1 and $Cmca$-12$-$BL2 obtained by vdW-DF1 both increase by density. But vdW-DF2 optimized molecular bond-length indicate that $Cmca$-12$-$BL1 and $Cmca$-12$-$BL2 decreases and increases by pressure, respectively. All the $H-H$ molecular bond-lengths in the $Cmca$ phase are identical and consequently one vibron can be observed in phonon DOS (Figure 4). The vdW-DF1 and vdW-DF2 predict that $Cmca$-BL increases by rising pressure. $Cmca$-BL is larger than $C2/c$ and $Cmca$-12 molecular bond-lengths and therefore the vibron frequency of the $Cmca$ is smaller than $C2/c$ and $Cmca$-12 structures.

Recently we have used many-body wave-function based quantum Monte Carlo methods to calculate excitonic and quasi-particle band gap and also electronic band-structure of the $C2/c$, $Pbcn$, and $P6_3/m$ phases[37]. We have discovered that many properties of solid molecular hydrogen are strongly correlated with $H-H$ molecular bond-length. For instance, the

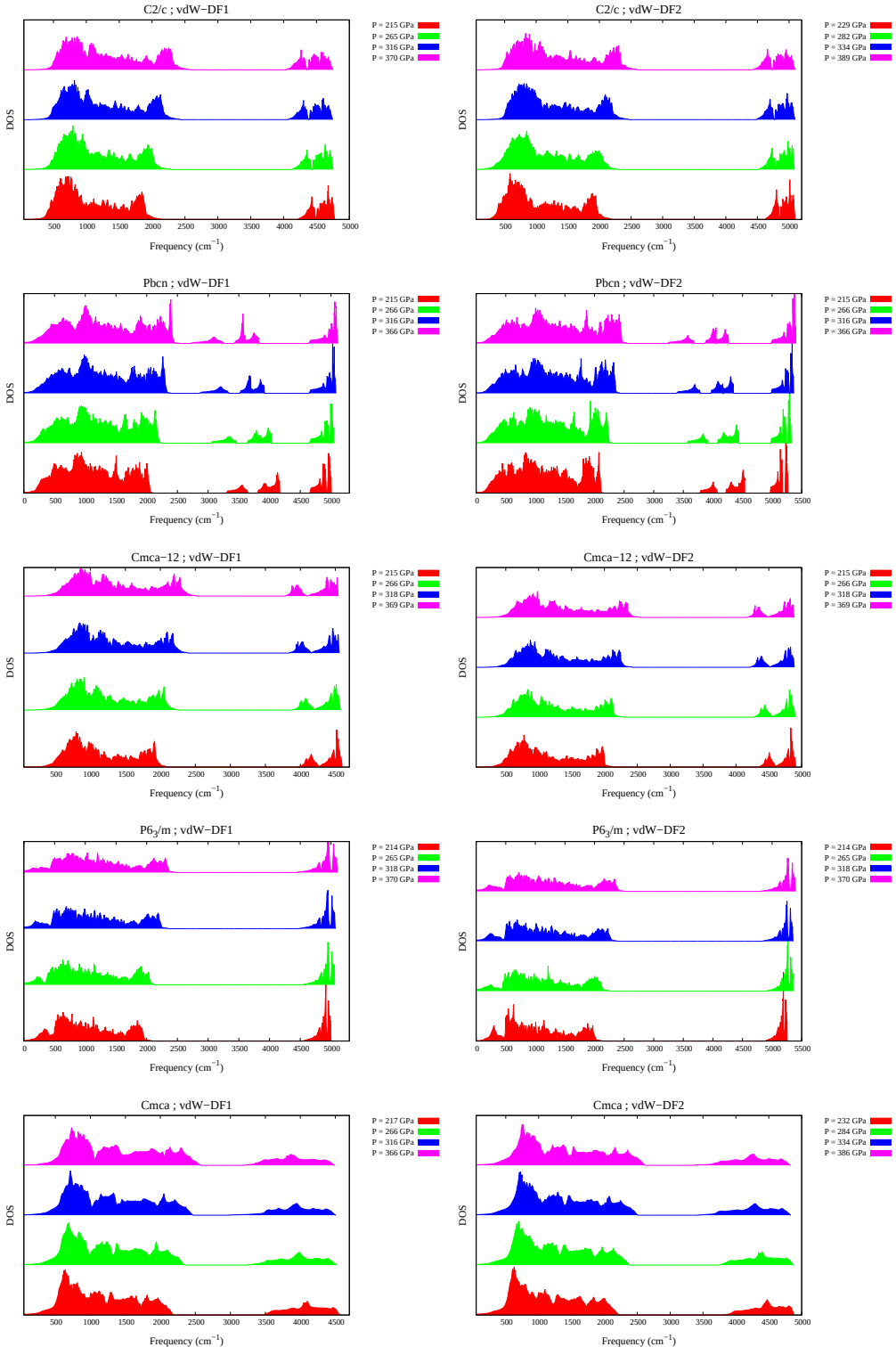


FIG. 3. (Color online) The phonon density of states of the $C2/c$, $Pbcn$, $Cmca$-12, $P6_3/m$, and $Cmca$ phases calculated using vdW-DF1 and vdW-DF2 functionals at four different pressures.

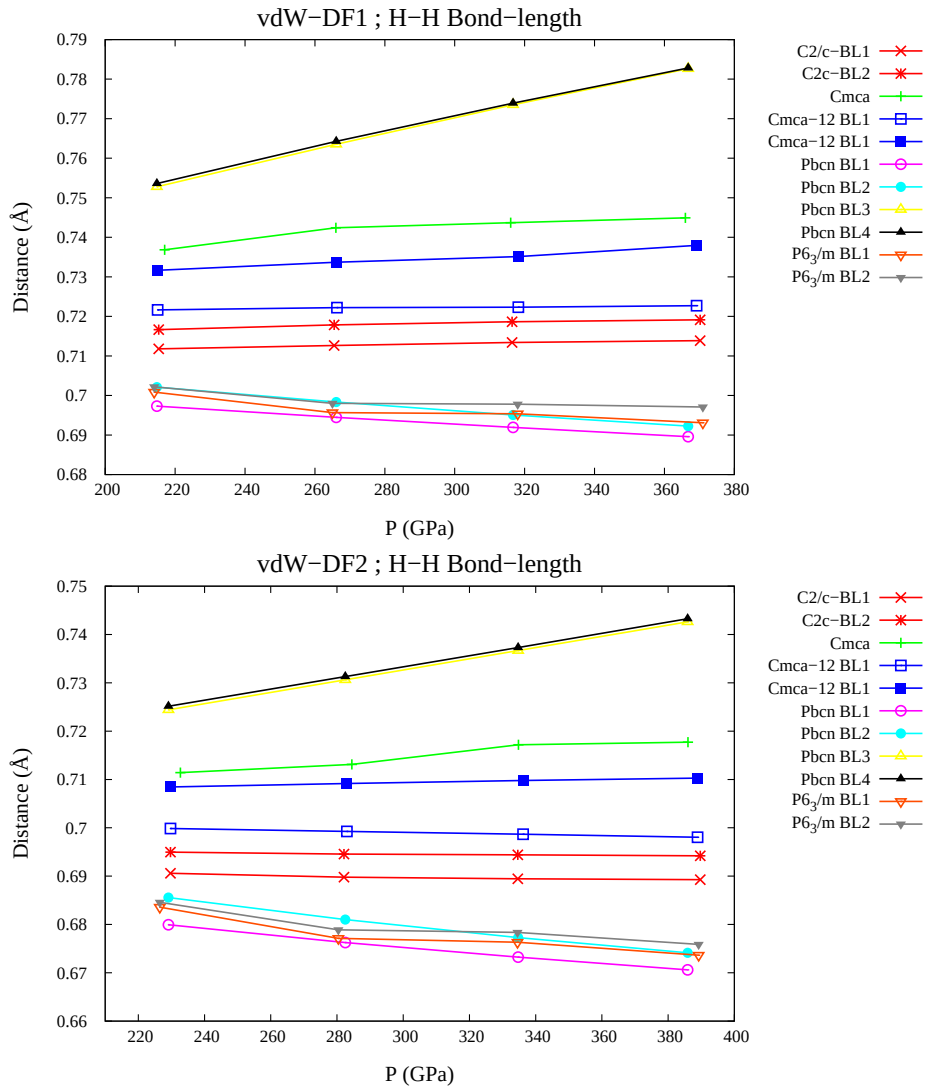


FIG. 4. (Color online) The optimized $H-H$ molecular bond-length (BL) of the $C2/c$, $Pbcn$, $Cmca$-12, $P6_3/m$, and $Cmca$ phases calculated using vdW-DF1 and vdW-DF2 functionals at different pressures. In the primitive unit cells of the $C2/c$, $Pbcn$, $Cmca$-12, $P6_3/m$, and $Cmca$ structures there are two, four, two, two, and one categories of $H_2$ molecules with different $H-H$ bond-lengths.

gradient of the $P6_3/m$ band gap with respect to molecular BL is $\sim$ 27.3 eV/$\mathring{A}$ independent of the XC functional. As illustrated in Figure 4, the twenty four $H_2$ molecules in the unit cell of the $Pbcn$ phase adopt four non-equivalent $H-H$ molecular bond-lengths, and thus four vibron frequencies are obtained. $Pbcn$−BL1 and $Pbcn$−BL2, which shorten with pressure are shorter than $Pbcn$−BL3 and $Pbcn$−BL4, which lengthen with pressure(Table

I). This behaviour correlates with the *Pbcn* phonon DOS where increasing the pressure reduces the two low vibron frequencies and increases two high vibron frequencies. The $P6_3/m$ structure has eight $H_2$ molecules per primitive unit cell with two inequivalent bond-lengths $P6_3/m-$BL1 and $P6_3/m-$BL2 with difference of $\sim 4m\mathring{A}$. VdW-DF1 and vdW-DF2 results indicate that $P6_3/m-$BL1 and $P6_3/m-$BL2 are reduced by increasing density.

The averaged molecular bond-length by vdW-DF1, which is defined as $BL_{ave} = 1/n \sum_i^n BL_i$ where n is the number of bond-lengths, of all the studied phases increase by pressure except the $P6_3/m$. vdW-DF2 calculations show that $BL_{ave}$ reduction of the $C2/c$ and $P6_3/m$ due to increasing the pressure are $1m\mathring{A}$ and $9m\mathring{A}$, respectively. Similar to vdW-DF1 results the $BL_{ave}$ of other structures calculated by vdW-DF2 are increases by dense. By increasing the pressure both low energy lattice phonon frequencies and high frequency vibron modes become larger. Decreasing the $P6_3/m$-$BL_{ave}$ with pressure causes an instability in the system which is also found from imaginary phonon frequencies. It should be noted that at high enough pressures molecular to atomic phase transition occurs. The Raman spectra and MD simulations suggest that phase IV is a mixture elongated $H_2$ dimers experiencing large pairing fluctuations, and unbound $H_2$ molecules[12]. This matches very well with the altering of *Pbcn* molecular bond-lengths with pressure. The $Pbcn-$BL1 and $Pbcn-$BL2 decrease with increasing the pressure whereas $Pbcn-$BL4 and $Pbcn-$BL3 dissociate by increasing the pressure. Benchmarking DFT-XC functionals for high pressure solid hydrogen using quantum Monte Carlo (QMC) simulations indicate that, at static level, optimized molecular bond-length for the $C2/c$ which is calculated by vdW-DF1 functional agrees with QMC results[26].

The molecular bond-length, which is also the nearest-neighbour distance, is strongly correlated with electronic energy band gap. We do not present DFT band gap results here as our recent extensive study of energy band gap of solid molecular hydrogen is reported in reference 37. At constant pressure, the $P6_3/m$ band gap is larger than other molecular phases. As it is shown in figure 4, the $P6_3/m-$BL$_{ave}$ is smaller than other studied structures. Shortening molecular bond-length localises the electrons and increase localised charge density and consequently, according to the band theory, opening the energy band gap is expected. Hence, a precise bond length is necessary for an accurate prediction of the properties of solid molecular phases. We propose a rule of thumb of *the shorter molecular bond-length the larger electronic band gap the higher vibron frequencies* which is independent of the XC

| vdW-DF1 | $C2/c$ | | $Cmca$ | $Cmca$-12 | | $Pbcn$ | | | | $P6_3/m$ | |
|---|---|---|---|---|---|---|---|---|---|---|---|
| P | BL1 | BL2 | BL | BL1 | BL2 | BL1 | BL2 | BL3 | BL4 | BL1 | BL2 |
| 215 | 0.71179 | 0.71664 | 0.73683 | 0.72164 | 0.73165 | 0.69731 | 0.70211 | 0.75279 | 0.75361 | 0.70085 | 0.70219 |
| 265 | 0.71265 | 0.71784 | 0.74240 | 0.72222 | 0.73371 | 0.69447 | 0.69833 | 0.76352 | 0.76427 | 0.69565 | 0.69802 |
| 316 | 0.71341 | 0.71865 | 0.74370 | 0.72233 | 0.73511 | 0.69193 | 0.69505 | 0.77351 | 0.77394 | 0.69537 | 0.69780 |
| 370 | 0.71386 | 0.71912 | 0.74491 | 0.72272 | 0.73795 | 0.68958 | 0.69224 | 0.78263 | 0.78283 | 0.69309 | 0.69707 |
| vdW-DF2 | | | | | | | | | | | |
| 230 | 0.69058 | 0.69496 | 0.71141 | 0.69985 | 0.70846 | 0.67994 | 0.68557 | 0.72442 | 0.72514 | 0.68358 | 0.68459 |
| 282 | 0.68979 | 0.69457 | 0.71311 | 0.69924 | 0.70916 | 0.67625 | 0.68102 | 0.73063 | 0.73129 | 0.67712 | 0.67888 |
| 335 | 0.68945 | 0.69440 | 0.71719 | 0.69868 | 0.70980 | 0.67324 | 0.67727 | 0.73666 | 0.73730 | 0.67633 | 0.67835 |
| 390 | 0.68927 | 0.69421 | 0.71771 | 0.69804 | 0.71029 | 0.67061 | 0.67413 | 0.74261 | 0.74325 | 0.67364 | 0.67587 |

TABLE I. Precise values of molecular bond-length in $\mathring{A}$ for the $C2/c$, $Cmca$, $Cmca$-12, $Pbcn$, and $P6_3/m$ structures calculated by vdW-DF1 and vdW-DF2 at various pressures (in GPa). First column shows the pressure (P) in GPa. Notice how the shorter bond lengths become shorter with pressure, while longer BLs become longer.

functional in DFT calculations study of high-pressure solid molecular hydrogen. We have recently calculated the *scissor operator* for solid molecular hydrogen structures and we have demonstrated that the *scissor operator* is also independent of DFT XC functional[29].

We also calculated active IR modes for the solid molecular phases, $C2/c$, $Pbcn$, $Cmca$-12, $P6_3/m$, and $Cmca$ structures which are calculated by vdW-DF1 and vdW-DF2 at four different pressures ( Figure 5 ). The main difference between vdW IR spectra and those simulated using conventional semi-local functionals is the position of peak. The position of IR peaks depends on the optimized BL predicted by XC functional. The gradient of IR peak with respect to BL is $\sim 14.95 \pm 0.5 (cm.m\mathring{A})^{-1}$ which is independent of pressure and is also identical for the studied molecular structures. It indicates that altering bond-length by $0.1\mathring{A}$, which equals to accuracy of DFT functionals in prediction of optimized BL for $H_2$ molecule, shifts the IR peak by $1495 \pm 5 (cm)^{-1}$. This value is almost same as the gap in phonon density of states.

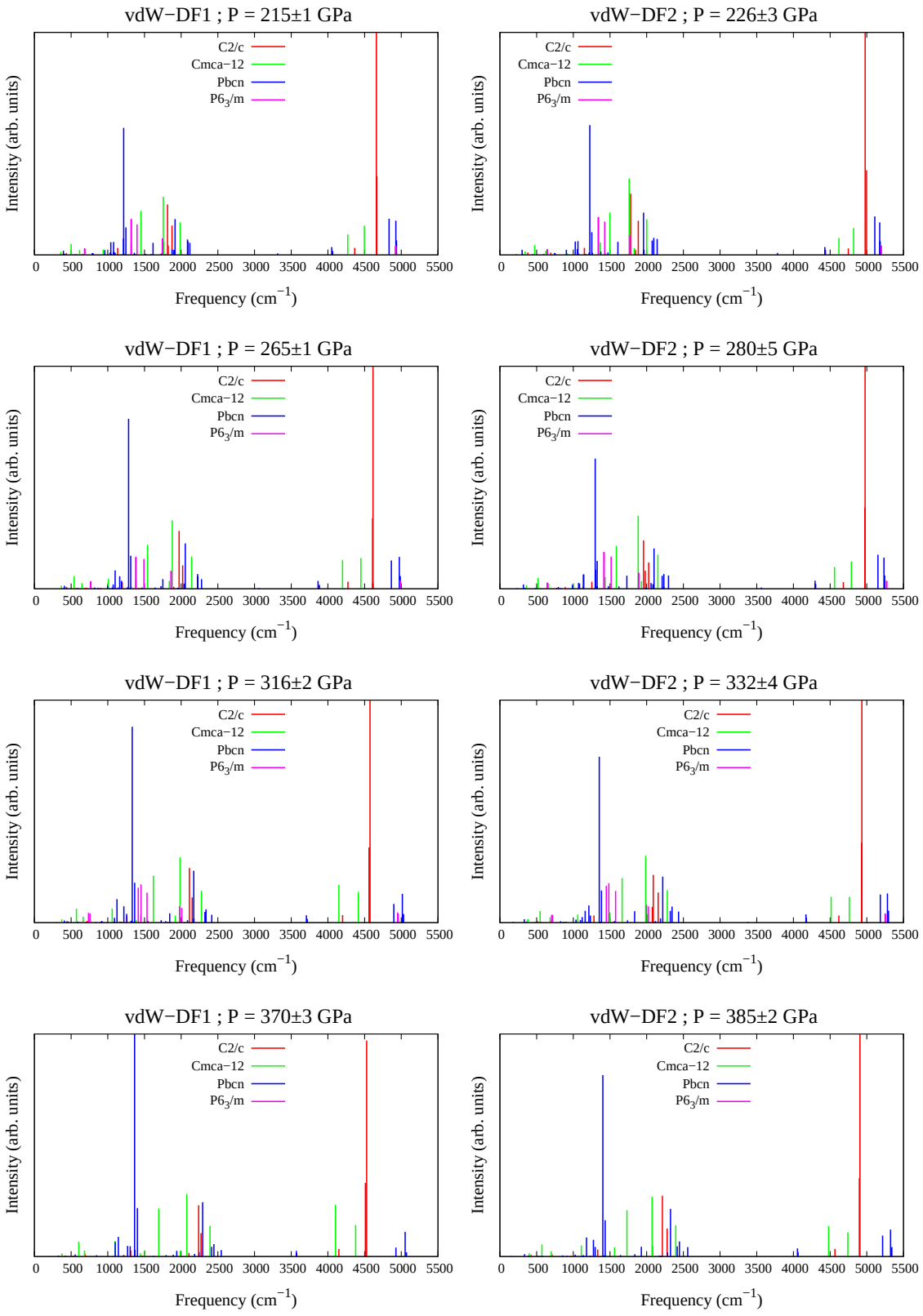


FIG. 5. (Color online) IR frequencies and relative intensities for the $C2/c$, $Pbcn$, $Cmca$-12, $P6_3/m$, and $Cmca$ phases calculated using vdW-DF1 and vdW-DF2 functionals at four different pressures.

### C. Finite temperature phase diagram

We calculated the quasiharmonic Gibbs free energy for high pressure solid molecular hydrogen phases utilising the vdW functionals. Figure 6 illustrates the Gibbs free energy as a function of pressure at T = 10, and 310 K. Lattice vibrations and zero point (ZP) contributions play a crucial role in determining phase boundaries. Our low-temperature vdW-DF1 phase diagram is rather similar to previous work with PBE. It predicts that the $C2/c$ is the most stable phase up to 289 GPa where it transforms to metallic $Cmca$ phase. Increasing the temperature to 310 K reduces the $C2/c$ to $Cmca$ phase transition pressure to 275 GPa. Comparing to previous DFT phase diagram results, this is the lowest DFT molecular insulator to molecular metallic phase transition pressure. vdW-DF1 phase diagram predicts that metallization of high-pressure solid hydrogen occurs through molecular-molecular phase transition at pressure below 300 GPa, whereas experiments[12,13,16,62,68] suggest that the metallization of solid hydrogen takes place at pressures larger than 350 GPa. Including the lattice dynamic contribution to the vdW-DF1 phase diagram increases the discrepancy between vdW-DF1 outcomes and experimental observations as well as our recently reported QMC results[37].

Our vdW-DF2 Gibbs free energy calculations (figure 6) indicate two low temperature phase transitions of $C2/c$ to $Pbcn$ at 291 GPa and $Pbcn$ to $Cmca$ at 402 GPa. Whatever functional is used, the effects of nuclear quantum and thermal vibrations play a crucial role in the stabilization of phase III and IV. Recent DFT calculations report a new hexagonal structure with $P6_122$ symmetry for phase III of solid molecular hydrogen, which is more stable than $C2/c$ at pressures below 200 GPa[63]. We suggest that two molecular insulator structures with molecular positions close to hcp could be stabilized above 200 GPa in the region ascribe to phase III: monoclinic $C2/c$ up to 291 GPa, and $Pbcn$ up to 402 GPa pressure. By increasing the temperature to T = 310 K the insulator $Pbcn$ to metallic $Cmca$ phase transition occurs at 366 GPa. Our previous QMC results[17] predict that molecular to atomic phase transition takes place at about 374 GPa. Our recent quasi-particle and excitonic band gap study[37] also suggests that band-gap closure of best candidates for solid molecular structures occurs within pressure range of 350-400 GPa. This work predicts that insulator to metallic phase transition happens at 366 GPa. Based on our extensive study of the metallisation of high pressure solid hydrogen, we conclude that all three scenarios

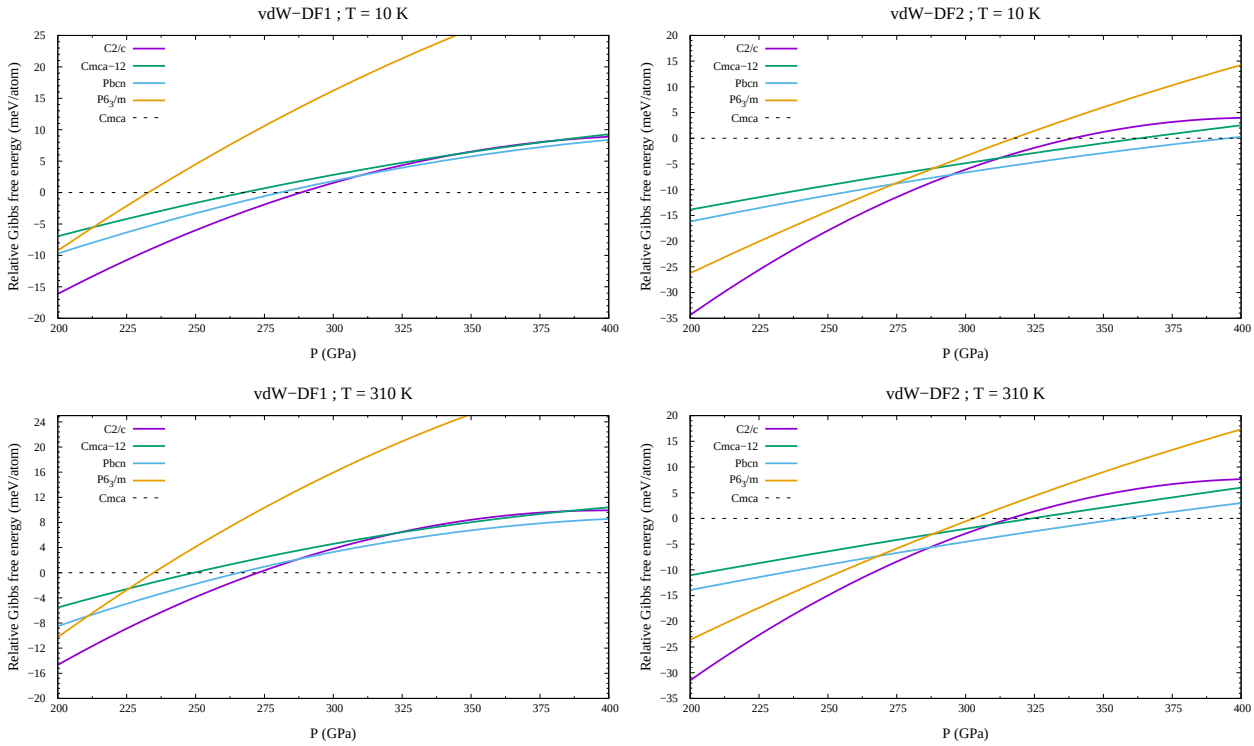


FIG. 6. (Color online) Relative Gibbs free energy per atom as a function of pressure at T = 10, and 310 K calculated using vdW-DF1 and vdw-DF2. The Gibbs free energy of molecular crystal structures are presented relative to the metallic *Cmca* structure.

of metallisation, which are molecular-atomic structural transformation, band-gap closure and insulator molecular to metallic molecular phase transition, indicate that solid hydrogen become a metal at pressure range of 350-400 GPa. This prediction agrees well with experiments[12,13,62].

Figure 7 illustrates temperature-pressure phase diagram for solid molecular hydrogen which is predicted by vdW-DF2. The metallisation transition to *Cmca* is strongly affected by quantum zero point fluctuations and occurs above 400GPa,consistent with experiment. Zero point fluctuations also destabilize $C2/c$ with respect to *Pbcn* around 300GPa with either functional. Increasing the temperature reduces the metal-insulator phase transition pressure. The stability of phase III, at room temperature has been observed experimentally[12]. The Raman and visible transmission spectroscopy measurements at 300 K and up to 315 GPa indicate the phase transformation to phase III around 200 GPa.

Finally we argue that the vdW-DF2 functional provides better results at high density limit than vdW-DF1 for the same reason that BLYP performs better than PBE. The GGA

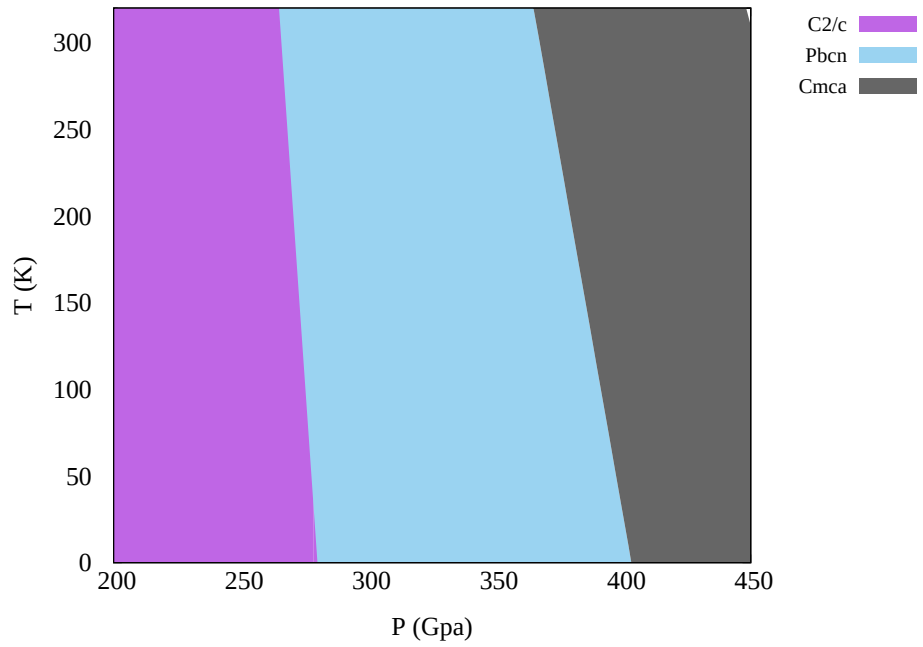


FIG. 7. (Color online) Predicted temperature-pressure phase diagram for solid molecular hydrogen obtained by vdW-DF2. The zero point fluctuations are the influential term in the Gibbs free energy calculations which stabilises the *Pbcn* and metallic *Cmca* phases. The main contribution to zero-point comes from the vibrons, while the thermal-phonon effects depend more on the lattice modes

functional, which is used in both vdW-DF1 and vdW-DF2, can be given by

$$E_x^{GGA}[n(\mathbf{r}), \nabla n(\mathbf{r})] = -(3/4)(3/\pi)^{1/3} \int d^3r n^{4/3} A_x^{GGA}(s) \tag{2}$$

where $s = (\nabla n)/(2k_F n)$, and $k_F = (3\pi^2 n)^{1/3}$ is the local Fermi wave vector. The PBE and revPBE enhancement factor formula , which is used in vdW-DF1, is

$$A_x(s) = 1 + \frac{\mu s^2}{1 + \mu s^2/\kappa} \tag{3}$$

where both PBE and revPBE use $\mu = 0.2195$ which correctly describes the low $s$ limit but and PBE and revPBE become insensitive to $s$ in the high-$s$ limit. For $H_2$ dimers, significant values of $s$ as large as 25 is obtained[61], which can yield spurious exchange attractions in PBE and vdW-DF1.

The PW86, which is almost linear in $s$, gives an enhancement factor proportional to $s^{2/5}$ at large $s$, and provides net repulsive interaction for exchange energy[64]. Detailed analysis

of GGA functionals[61,64] indicate that PW86 (as used in vdW-DF2) is the best for systems dominated by large $s$ such as high pressure hydrogen.

## IV. CONCLUSION

We have employed non-local vdW functionals to revisit the phase diagram of high-pressure solid hydrogen within pressure range of $200 < P < 450$ GPa. We studied the best candidates for phase III previously discovered by structure searching using the PBE approach. In phase III the $H_2$ bond weakens with pressure as electrons delocalize, and there is competition between insulating and metallic, molecular and atomic structure. Consequently, the cancellation of exchange-correlation errors which typically allows DFT to give accurate energy differences is most sorely tested here. In previous work it was shown that, compared with experiment and QMC calculation, PBE obtains over-long BLs, too-low vibron frequencies, and too-low transition pressure to the molecular metallic phase ($Cmca$). By considering a range of XC functionals, we have shown that these failings are all related.

To examine the importance of the long-range vdW interactions in solid molecular structures of high-pressure hydrogen, we made use of two widely applied vdW functionals of vdW-DF1 and vdW-DF2 to calculate static-enthalpy and finite-temperature dynamic Gibbs free energy as functions of pressure. The vdW-DF1 gives erroneous results similar to PBE, while vdW-DF2 gets bond lengths, frequencies and transition pressures close to QMC and experimental results.

The distinguishing feature of the more successful functionals is the treatment of semi-local exchange rather than in inclusion of vdW. In particular those functionals which correctly fit the limit of high charge density gradient give better-defined molecules. Interestingly, this effect is most pronounced in the molecular metallic phase ($Cmca$) which is overly stable in PBE due to the low vibron frequency and consequent low zero-point energy.

The sensitivity of the metallization pressure to choice of XC functional is likely to be a feature of all hydrogen phases. Our results suggest that previous DFT calculations of metallization pressure, including the metallization of the liquid, will have an uncertainty of order $\pm 100$ GPa, with the widely used PBE functional giving especially low values.

## V. ACKNOWLEDGMENTS

This work was supported by the European Research Council (ERC) Grant "Hecate" reference No. 695527. Computing facilities were provided through DECI-13 PRACE project "QMCBENZ15" and the Dutch national supercomputer Cartesius. S. Azadi acknowledges useful discussions with Ĕ. D. Murray. GJA acknowledges support from EPSRC (UKCP grant K01465X) and a Royal Society Wolfson fellowship.

* s.zadi@ic.ac.uk ; sam.azadi@ed.ac.uk

[1] E. Wigner and H. B. Huntington, J. Chem. Phys. **3**, 764 (1935).

[2] N. W. Ashcroft, Phys. Rev. Lett. **21**, 1748 (1968).

[3] S. A. Bonev, E. Schwegler, T. Ogitsu, and G. Galli, , Nature **431**, 669 (2004).

[4] H. K. Mao and R. J. Hemley, Rev. Mod. Phys. **66**, 671 (1994).

[5] V. L. Ginzburg, Phys. Usp. **42**, 353 (1999).

[6] E. Gregoryanz, A. Goncharov, K. Matsuishi, H-K. Mao, and R. Hemley, Phys. Rev. Lett. **90**, 175701 (2003).

[7] V. Kechin, Phys. Rev. B **65**, 052102 (2001).

[8] M. I. Eremets, and I. Troyan, JETP Lett. **89**, 174 (2009).

[9] J. Kohanoff, S. Scandolo, G.L. Chiarotti, and E. Tosatti, Phys. Rev. Lett. **78**, 2783 (1997).

[10] J. Kohanoff, S. Scandolo, S. de Gironcoli, and E. Tosatti, Phys. Rev. Lett. **83**, 4097 (1999).

[11] M. I. Eremets and I. A. Troyan, Nat. Mater. **10**, 927 (2011).

[12] R. T. Howie, C. L. Guillaume, T. Scheler, A. F. Goncharov, and E. Gregoryanz, Phys. Rev. Lett. **108**, 125501 (2012).

[13] R. T. Howie, I. B. Magdău, A. F. Goncharov, G. J. Ackland, and E. Gregoryanz, Phys. Rev. Lett. **113**, 175501 (2014).

[14] R. T. Howie, P. Dalladay-Simpson, and E. Gregoryanz, Nat. Mater. **14**, 495 (2015).

[15] P. Dalladay-Simpson, R. T. Howie, and E. Gregoryanz, Nature **529**, 63 (2016).

[16] C. S. Zha, Z. Liu, and R. J. Hemley, Phys. Rev. Lett. **108**, 146402 (2012).

[17] S. Azadi, B. Monserrat, W. M. C. Foulkes, and R. J. Needs, Phys. Rev. Lett. **112**, 165501 (2014).

[18] M. Städele and R. Martin, Phys. Rev. Lett. **84**, 6070 (2000).

[19] K. A. Johnson and N. W. Ashcroft, Nature **403**, 632 (2000).

[20] C. J. Pickard and R. J. Needs, Nat. Phys. **3**, 473 (2007).

[21] C. J. Pickard, M. Martinez-Canales, and R. J. Needs, Phys. Rev. B **85**, 214114 (2012).

[22] A. F. Goncharov, J. S. Tse, H. Wang, J. Yang, V. V. Struzhkin, R. T. Howie, and E. Gregoryanz, Phys. Rev. B **87**, 024101 (2013).

[23] I. B. Magdău and G. J. Ackland, Phys. Rev. B **87**, 174110 (2013).

[24] I. I. Naumov, R. E. Cohen, and R. J. Hemley, Phys. Rev. B **88**, 045125 (2013).

[25] M. A. Morales, J. M. McMahon, C. Pierleoni, and D. M.Ceperley, Phys. Rev. B **87**, 184107 (2013).

[26] R. C. Clay, J. Mcminis, J. M.McMahon, C. Pierleoni, D. M. Ceperley, and M. A. Morales, Phys. Rev. B **89**, 184106 (2014).

[27] S. Azadi and T. D. Kühne, JETP letters **95**, 449 (2012).

[28] R. Singh, S. Azadi, and T. D. Kühne, Phys. Rev. B **90**, 014110 (2014).

[29] S. Azadi and W. M. C. Foulkes, Phys. Rev. B **88**, 014115 (2013).

[30] I. B. Magdău and G. J. Ackland, Phys. Rev. Lett. **118** 145701 (2017).

[31] R. P. Dias, O. Noked, and I.F. Silvera, Phys. Rev. Lett. **116**, 145501, (2016).

[32] W. M. C. Foulkes *et al.*, Rev. Mod. Phys. **73**, 33 (2001).

[33] S. Azadi and W. M. C. Foulkes, J. Chem. Phys. **143**, 102807 (2015).

[34] S. Azadi and R. E. Cohen, J. Chem. Phys. **143**, 104301 (2015).

[35] S. Azadi, W. M. C. Foulkes, and T. D. Kühne, New J. Phys. **15**, 113005 (2013).

[36] N. D. Drummond *et al.*, Nat. Comm. **6**, 7794 (2015).

[37] S. Azadi, N. D. Drummond, and W. M. C. Foulkes, Phys. Rev. B **95**, 035142 (2017).

[38] G. J. Ackland and I. B. Magdău Cogent Physics **2** 1049477 (2015)

[39] I. B. Magdău, M. Marqués, B. Borgulya, and G. J. Ackland, Phys. Rev. B **95**, 094107 (2017).

[40] B. Santra, J. Klimeš, D. Alfè, A. Tkatchenko, B. Slater, A. Michaelides, R. Car, and M. Scheffler, Phys. Rev. Lett. **107** 185701 (2011).

[41] S. Azadi and R. E. Cohen, J. Chem. Phys. **145**, 064501 (2016).

[42] W. L. Vos, L. W. Finger, R. J. Hemley, J. Z. Hu, H. K. Mao, and J. A. Schouten, Nature **358**, 46 (1992).

[43] M. D. Knudson, M. P. Desjarlais, A. Becker, R. W. Lemke, K. R. Kochrane, M. E. Savage, D. E. Bliss, T. R. Mattsson, and R. Redmer, Science **348** 1455 (2015).

[44] M. Dion, H. Rydberg, E. Schröder, D. C. Langreth, and B. I. Lundqvist, Phys. Rev. Lett. **92**, 246401 (2004).

[45] T. Thonhauser, S. Zuluaga, C.A. Arter, K. Berland, E. Schröder, and P. Hyldgaard, Phys. Rev. Lett. **115**, 136402 (2015).

[46] K. Lee, Ĕ. D. Murray, L. Kong, B. I. Lundqvist, and D. C. Langreth, Phys. Rev. B **82**, 081101(R) (2010).

[47] J. Klimeš, D. R. Bowler, and A. Michaelides, Phys. Rev. B **83**, 195131 (2011).

[48] J. Klimeš, and A. Michaelides, J. Chem. Phys. **137**, 120901 (2012).

[49] Y. Akahama, H. Kawamura, N. Hirao, Y. Ohishi and K. Takemura, J. Phys: Conference Series **215**, 012056 (2010)

[50] P. Giannozzi *et al.*, J. Phys.: Condens. Matt. **21**, 395502 (2009).

[51] J. P. Perdew, K. Burke, and M. Ernzerhof, Phys. Rev. Lett. **77**, 3865 (1996).

[52] S. Baroni, S. de Gironcoli, and A. Dal Corso, Rev. Mod. Phys. **73**, 515 (2001).

[53] J. P. Perdew, and Y. Wang, Phys. Rev. B **45**, 13244 (1992).

[54] Y. Zhang and W. Yang, Phys. Rev. Lett. **80**, 890 (1998).

[55] J. P. Perdew and Y. Wang, Phys. Rev. B **33**, 8800(R) (1986).

[56] E. D. Murray, K. Lee, and D. C. Langreth, J. Chem. Theory Comput. **5**, 2754 (2009).

[57] H. Rydberg, M. Dion, N. Jacobson, E. Schröder, P. Hyldgaard, S. I. Simak, D. C. Langreth, and B. I. Lundqvist, Phys. Rev. Lett. **91**, 126402 (2003).

[58] C. Lee, W. Yang, and R. G. Parr, Phys. Rev. B **37**, 785 (1988).

[59] Perdew, J. P., Ruzsinszky, A., Csonka, G. I., Vydrov, O. A., Scuseria, G. E., Constantin, L. A. and Burke, K. Phys. Rev. Lett. **100**, 136406 (2008)

[60] V. Polo, E. Kraka, and D. Cremer, Mol. Phys. **100**, 1771 (2002).

[61] E. D. Murray, K. Lee, and D. C. Langreth, J. Chem. Theory Comput. **5**, 2754 (2009).

[62] P. Loubeyre, F. Occelli, and R. LeToullec, Nature (London) **416**, 613 (2002)

[63] B. Monserrat, R. J. Needs, E. Gregoryanz, and C. J. Pickard, Phys. Rev. B **94**, 134101 (2016)

[64] F. O. Kannemann, and A. D. Becke, J. Chem. Theory Comput. **5**, 719 (2009)

[65] C. J. Pickard, and R. J. Needs, Physica Status Solidi (b) **246**, 536 (2009)

[66] H. Liu, L. Zhu, W. Cui and Y. Ma, J. Chem. Phys. **137**, 074501 (2012)

[67] H. Liu, and Y. Ma, Phys. Rev. Lett. **110**, 025903 (2013)

[68] R. P. Dias, and I. F. Silvera, Science **355**, 715 (2017)